Earth and Planetary Science Letters 547 (2020) 116462

Contents lists available at ScienceDirect

Earth and Planetary Science Letters

www.elsevier.com/locate/epsl

Astrochronology of the Ediacaran Shuram carbon isotope excursion, Oman

Zheng Gong [a,*], Mingsong Li [b]

[a] Department of Earth and Planetary Sciences, Yale University, New Haven, CT 06511, USA
[b] Department of Geosciences, Pennsylvania State University, University Park, PA 16802, USA

ARTICLE INFO

Article history:
Received 11 February 2020
Received in revised form 14 June 2020
Accepted 3 July 2020
Available online 27 July 2020
Editor: L. Derry

Keywords:
Ediacaran
Nafun Group
gamma ray
Shuram excursion
astrochronology

ABSTRACT

The Ediacaran is a highly dynamic period in terms of large perturbations in Earth's atmosphere, biosphere, and climate. Among these perturbations, a pronounced negative carbon isotope excursion, known as the Shuram excursion (SE), is characterized by the most depleted $\delta^{13}C$ values (-12‰) that have ever been observed in the geological record. A poorly determined chronostratigraphic framework makes the SE difficult to correlate and compare globally. Therefore, it is hard to study the potential connection between the SE and coeval climate and biological variations. Here, we present a high-resolution astrochronological study of the Ediacaran Shuram and Buah Formations, Nafun Group, Oman, in which the SE is reported for the first time. Power spectral analysis of the 600-m long gamma ray log of the Miqrat-1 Well shows that a hierarchy of astronomically-forced climate cycles (eccentricity, obliquity, and precession) is accurately-preserved. Using multiple statistical tests, we constructed a sedimentation rate variation profile that covers the entire SE, which is characterized by low rates in shale-dominated layers and high rates in shale-carbonate interbedded layers. The duration of the SE in Oman is suggested to be 7.7 ± 0.2 Myr, which agrees with estimates from South Australia, South China, and the United States. An identical duration of the SE supports its global synchroneity and indicates a primary origin of the depleted $\delta^{13}C$ values. Combined with the newly proposed termination age (562.5 ± 1.1 Ma) of the SE, our astrochronological results suggest that the onset age of the excursion is 570.2 ± 1.1 Ma. The astrochronology of the SE delineates the tempo of the excursion, with a rapid decrease (~ 1 Myr) from the onset to its isotopic nadir followed by a more gradual recovery (~ 6–7 Myr) towards the termination. The new chronostratigraphic framework permits further investigations of the potential causal links between the global carbon cycle and the widespread glaciation, the oceanic oxygenation, and the biological diversification in Ediacaran time.

1. Introduction

The Ediacaran Period (ca. 635-541 Ma; Knoll et al., 2006) is one of the most dynamic time intervals in Earth's history, which is marked by the stepwise buildup of oxygen in the ocean and atmosphere (Lyons et al., 2014), anomalous behavior of the geomagnetic field (Meert et al., 2016), multiple perturbations of the global carbon cycle (Halverson et al., 2005), and the emergence and diversification of multicellular organisms (Xiao and Laflamme, 2009). Shifts in oceanic carbon isotopic compositions preserved in carbonate rocks are closely associated with Earth's climate and biological evolution (Kump and Arthur, 1999). A pronounced negative $\delta^{13}C$ excursion has been globally observed (Fig. 1A) in mid-Ediacaran strata, which is broadly contemporaneous with the rise of Ediacara biota (McFadden et al., 2008; Xiao and Laflamme, 2009). This carbon isotope excursion, known as the Shuram excursion (SE), is characterized by extremely depleted $\delta^{13}C$ values (-12‰) and a prolonged (hundreds of meters) stratigraphic persistence (Grotzinger et al., 2011). Although a number of mechanisms have been proposed to explain its origin, it is still highly debated whether this excursion is a primary record of global ocean chemistry or merely a diagenetic overprint (Grotzinger et al., 2011). On the one hand, the depleted $\delta^{13}C$ values challenge the conventional view of global carbon isotope mass balance (Kump and Arthur, 1999), on the other hand, the lack of robust biological and geological markers makes the age of the SE poorly determined, hampering the worldwide correlation and comparison of this event.

A primary origin would require the global synchroneity of the excursion, that is, the age and the duration of the SE should be identical in its worldwide exposures. However, both the age and

* Corresponding author.
E-mail address: z.gong@yale.edu (Z. Gong).

https://doi.org/10.1016/j.epsl.2020.116462
0012-821X/

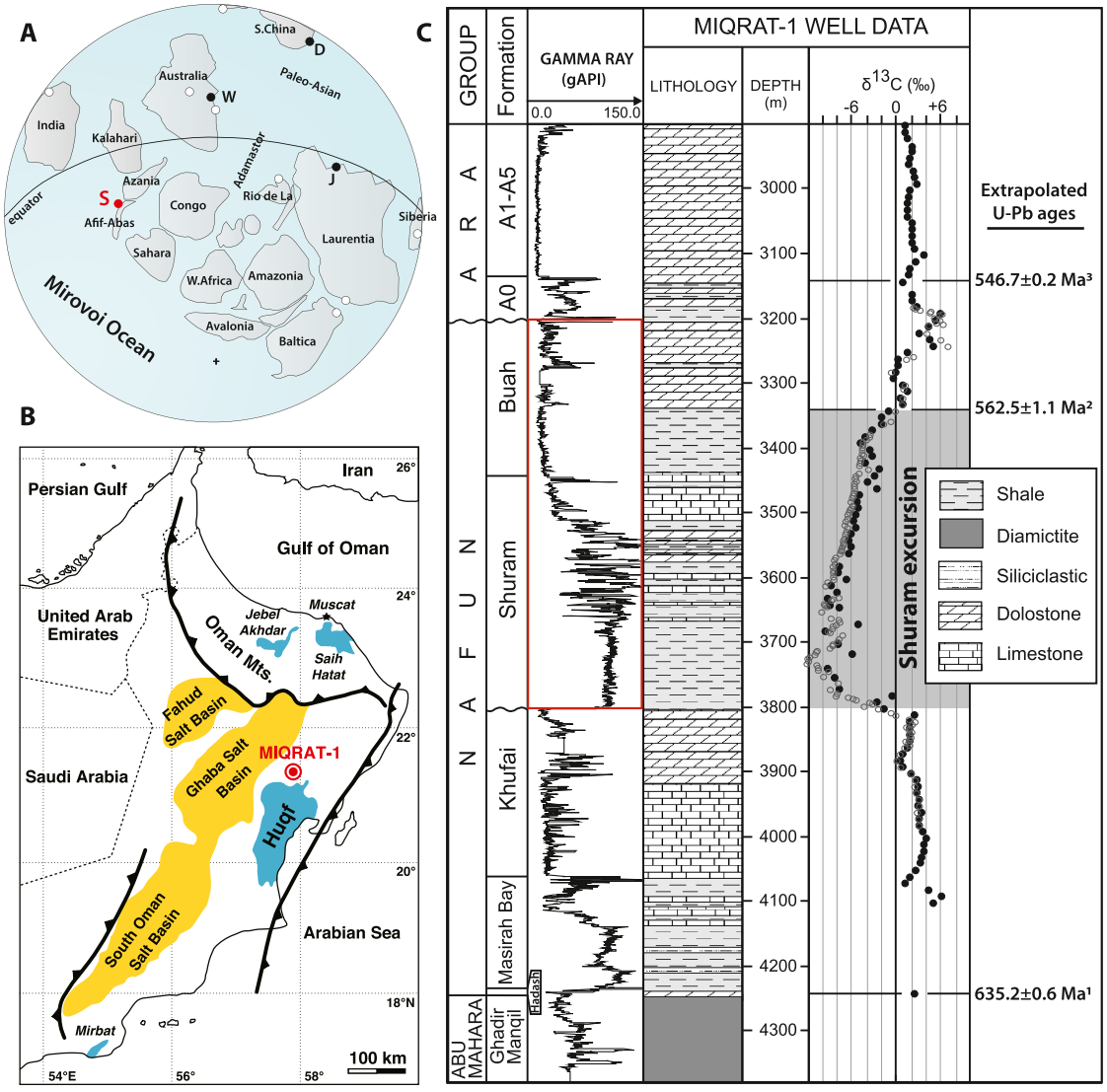

Fig. 1. (A) Paleogeographic map showing the exposures of the Shuram excursion (modified from Grotzinger et al., 2011). Black and red circles represent key sections with astrochronological constraints. White circles are potential sections of the excursion. S = Shuram Formation, Oman, W = Wonoka Formation in the Flinders Ranges, South Australia, D = Doushantuo Formation, South China, J = Johnnie Formation in the Death Valley, USA. Ediacaran paleogeography is reconstructed by Pisarevsky et al. (2008). (B) Geologic map of Oman (modified from Lee et al., 2013). Blue and yellow regions are Neoproterozoic strata exposures and salt basins, respectively. Location of the Miqrat-1 Well is shown as a red circled dot. (C) Lithology and raw GR log of the Miqrat-1 Well (modified from Bowring et al., 2007). Filled and open circles represent carbon isotope data from Burns and Matter (1993) and Fike et al. (2006), respectively. Red box shows the GR data used in this study. U-Pb zircon ages are from (1) Condon et al. (2005), (2) Canfield et al. (2020), and (3) Bowring et al. (2007). Stratigraphic levels of the U-Pb ages are inferred from chemostratigraphic correlation. (For interpretation of the colors in the figure(s), the reader is referred to the web version of this article.)

the duration of the SE are highly debated. Based on an ID-TIMS U-Pb zircon age from South China, the termination age of the SE is considered to be 551.1 ± 0.7 Ma (Condon et al., 2005). However, this age is challenged by Zhou et al. (2018), which argues that the SE in South China is stratigraphically below a 557 ± 3 Ma K-bentonite layer, meaning that the SE is much older than previously envisaged. A recent U-Pb age from the Trepassey Formation in Newfoundland suggests that the termination age of the SE is 562.5 ± 1.1 Ma (Canfield et al., 2020). By stratigraphic correlation with sections in Newfoundland, Pu et al. (2016) propose that the SE is younger than the ca. 580 Ma Gaskiers glaciation. Yet, there are no absolute ages that precisely date the onset age of the SE. Additionally, the duration of the SE has been inferred by different approaches. Basin thermal subsidence models have suggested a 6 Myr (Witkosky and Wernicke, 2018) or even a 50 Myr duration (Le Guerroué et al., 2006). Geochemical models could reproduce such a negative excursion over a period as little as 1 Myr (Bjerrum and Canfield, 2011) or as long as 10–30 Myr (Miyazaki et al., 2018). These estimates are incompatible, and the resolution of both the age and the duration is too low to determine if the SE is globally synchronous.

Astronomically-forced climate cycles (eccentricity, obliquity, and precession) that are encoded in sedimentary sequences can be retrieved from paleoclimate proxies and utilized to provide a continuous, high-resolution astrochronology at a decamillennial time scale. Using rock magnetic records of astronomical cycles, the duration of the SE has been estimated from exposures in South Australia, South China, and the United States (Fig. 1A; Minguez et al., 2015; Minguez and Kodama, 2017; Gong et al., 2017, 2019). These exposures lie paleogeographically in somewhat restricted Paleo-Asian and Adamastor Oceans (Fig. 1A). However, the most complete and representative section of the SE in Oman, which is located in the apparently expansive Mirovoi Ocean, has not yet been investigated (Fig. 1A). Here, we report a detailed astrochronological study of the Ediacaran Shuram and Buah Formations of the Nafun Group, Oman, in order to provide an astronomically-

calibrated time scale for the SE. Comparison with studies from other exposures will test the global synchroneity of the SE, and help understand its relationship with the climate and biological changes in Ediacaran time.

2. Geological setting

Oman provides a continuous record of the Ediacaran strata, known as the Nafun Group, which is broadly exposed in high topographic regions, e.g., the Oman Mountains in the north, the Huqf area in the middle, and the Mirbat area in the south (Fig. 1B; Gorin et al., 1982). Taking advantage of numerous oil wells, the Ediacaran strata have been well characterized and correlated across the entire basin (Gorin et al., 1982). The oldest sedimentary rocks are the Cryogenian diamictites and shales, namely the Abu Mahara Group, which lie unconformably on top of the ca. 800 Ma basement crystalline rocks (Fig. 1C). The uppermost glaciogenic sequence of the Abu Maraha Group is thought to be equivalent to the ca. 635 Ma Marinoan Snowball Earth event (Condon et al., 2005). Following that, the Ediacaran Nafun Group is over 1 km thick and starts with the cap dolostones (Hadash Formation) in the lowermost part (Fig. 1C). Upsection, the Nafun Group is further divided into the Masirah Bay Formation (shales), the Khufai Formation (carbonates), the Shuram Formation (shales and carbonates), and the Buah Formation (shales and carbonates). Between the Khufai and Shuram Formations is a disconformity. The Nafun Group documents important geobiological and geochemical records. For instance, a variety of *acritarchs* have been distinguished (Butterfield and Grotzinger, 2012). Burns and Matter (1993) first reported a pronounced negative carbon isotope excursion in the Shuram and Buah Formations in multiple sections across the basin. Those workers noticed that the $\delta^{13}C$ values drop sharply from +2 to -4‰ at the Khufai-Shuram boundary, reach to the nadir (-12‰) in the middle of the Shuram Formation, then gradually shift in a positive direction, and finally return back to pre-excursion values (+4‰) in the middle of the Buah Formation (Fig. 1C). This $\delta^{13}C$ excursion was then named after the Shuram Formation. Afterwards, similar events have been reported globally, including sections in South Australia (Calver, 2000), South China (Condon et al., 2005), and the United States (Corsetti and Kaufman, 2003; Fig. 1A). Above the Nafun Group is another disconformity, which is overlain by the Ara Group (carbonates and evaporites) that occupies the youngest part of the Ediacaran and extends through the Cambrian. Volcanic ash layers in the Ara Group yield several precise U-Pb zircon ages, which constrain the lowermost strata of the group to be 546.7 ± 0.2 Ma (Fig. 1C; Bowring et al., 2007). Between the ca. 635 Hadash cap dolostones and the ca. 547 Ma Ara carbonates, there is essentially no absolute age (Fig. 1C). Large gaps between the sporadic radiometric ages lead to a poorly developed chronostratigraphy, and an incomplete understanding of the geobiological and geochemical history of the Nafun Group.

3. Methods

Gamma ray (GR) logging is routinely used for lithological characterization. Concentration of naturally-occurring radioactive materials (e.g. clay minerals that are enriched in K, U, and Th) measured by GR could reflect changes in lithology, which is controlled by the depositional environment and the terrestrial input. Previous work shows that GR is among the most sensitive paleoclimate proxies for preserving astronomically-forced climate signals (Li et al., 2019b). Climate change modulated by astronomical cycles can affect monsoon intensities and runoff rates, or cause sea level fluctuations, which leads to the variation of clay mineral deposition, and eventually affects the GR values. GR logs have been successfully used in many astrochronological studies in the Phanerozoic (e.g., Li et al., 2019b).

The Miqrat-1 Well in the Huqf area was chosen for this study because it is the most representative and complete section of the Ediacaran strata in Oman and its carbon isotope data delineates the SE in detail (Fig. 1C; Burns and Matter, 1993; Fike et al., 2006). GR data of the Miqrat-1 Well was obtained by the Petroleum Development Oman (PDO; Forbes et al., 2010). The GR series has a high sampling resolution and completely covers the Nafun Group (Fig. 1C). We selected the 3800–3200 m segment of the GR series that includes the entire 460 m long SE (Fig. 1C). The raw GR series was linearly interpolated to get an evenly spaced sampling interval (0.15 m). Log-transformation was applied to stabilize the variance of GR values (Weedon, 2005). Then, we performed the wavelet transform (Torrence and Compo, 1998) to determine the distribution of strong cycling signals throughout the GR series. After that, we removed an 80 m 'loess' (local regression using weighted linear least squares and a second-degree polynomial model) long-term trend. Power spectral analysis was performed using the 2π multitaper method (MTM; Thomson, 1982). Robust red noise (Mann and Lees, 1996) was calculated in order to determine significant spectral peaks. The correlation coefficient (COCO) method was used to estimate the optimal sedimentation rate (Li et al., 2018). Evolutionary correlation coefficient (eCOCO) analysis was conducted to track variations in sedimentation rate through the GR series (Li et al., 2018). Both COCO and eCOCO analyses evaluated sedimentation rates ranging from 2 to 20 cm/kyr with a step increment of 0.1 cm/kyr by 2000 Monte Carlo simulations. The La2004 astronomical model was used for the periodicities of eccentricity (long eccentricity 405 kyr; short eccentricity 125 and 95 kyr; Laskar et al., 2004; Table 1). We used the estimates mainly from Waltham (2015) to get solutions for periodicities and the associated uncertainties of obliquity and precession at ca. 560 Ma (i.e., obliquity 31.8 ± 4.3 kyr; precession 20.2 ± 1.7, 19.2 ± 1.6, 16.8 ± 1.2, and 16.6 ± 1.2 kyr; Table 1). In addition, periodicities of obliquity and precession in Berger and Loutre (1994)'s model were also used as a comparison (Table 1). Numerical analyses were made using the Acycle 2.0 software (Li et al., 2019a).

4. Results

4.1. Power spectral analysis and sedimentation rate

Generally, GR values show a strong lithological dependence. GR values are consistently high in shale layers and low in carbonate layers, and change abruptly at lithological boundaries and unconformities (Fig. 1C). The wavelet transform, without any detrending and filtering, yields definitive cycling at ~ 32 m in 3650–3400 m and in 3350–3200 m (Fig. 2D). An ~ 8 m cycle is also noticed in 3670–3440 m. Instead, signals in 3800–3670 m, and around 3360 m are relatively weak compared to the rest of the series (Fig. 2D). The cycling pattern in the GR series detected by the wavelet transform is broadly consistent with lithology (Fig. 2), implying sedimentation rate variations throughout the section.

In consideration of both the results of wavelet transform and lithological variations, the GR series was subdivided into 4 intervals (i.e., 3800-3670 m, 3670–3440 m, 3440–3340 m, and 3340–3200 m) for the MTM spectral analysis (Fig. 2). A hierarchy of significant spectral peaks above the 95% confidence level was revealed in the power spectra (Fig. 3; Table 1). Specifically, Interval 1 has significant peaks with wavelengths of 19.7, 5.7, 3.9, 2.6, 2.3, 1.9, and 1.5 m. Interval 2 is dominated by peaks with wavelengths of 31.4, 8.7, 7.1, 5.0, 4.0, 3.0, 2.1, 1.9, 1.5, 1.4, 1.3, and 1.2 m. Interval 3 has peaks with wavelengths of 23.8, 6.7, 5.6, 2.9, 2.4, 2.0, 1.8, 1.4, and 1.2 m. Interval 4 is dominated by peaks with wavelengths of 31.6, 8.5, 7.4, 4.1, 3.3, 2.6, 1.7, and 1.6 m. Peaks at ~ 32 m and

Table 1
Astronomical periodicities at 560 Ma and cyclicities in the Shuram and Buah GR series.

Term	Periodicity (kyr)		GR series cyclicity (m)			
	Waltham (2015)	Berger and Loutre (1994)	Interval 1	Interval 2	Interval 3	Interval 4
Long eccentricity[a]	405	405	19.7	31.4	23.8	31.6
Short eccentricity[a]	125	125	5.7	8.7	6.7	8.5
	95	95	3.9	7.1	5.6	7.4
Long obliquity[b]	54	54	2.6	5.0	2.9	4.1
			2.3	4.0	2.4	3.3
			1.9	3.0		
Obliquity	31.8 ± 4.3	32.7-27.5	1.5	2.1	2.0	2.6
				1.9	1.8	
Precession	20.2 ± 1.7	18.1-15.5	–	1.5	1.4	1.7
	19.2 ± 1.6			1.4	1.2	1.6
	16.8 ± 1.2			1.3		
	16.6 ± 1.2			1.2		
Ratio	22 : 6 : 3 : 1.7 : 1	22 : 6 : 3 : 1.6 : 0.9	22 : 5.4 : 2.5 : 1.7 : –	22 : 5.5 : 2.8 : 1.4 : 0.9	22 : 5.7 : 2.4 : 1.7 : 1.2	22 : 5.5 : 2.3 : 1.8 : 1.1
Sedimentation rate (cm/kyr)	–	–	4.8	7.2	5.9	7.3

[a] From Laskar et al. (2004).
[b] From Hinnov (2013).

$\sim$ 8 m in the power spectra of Intervals 2 and 4 correspond to the signals observed in wavelet transform (Fig. 2D).

We calculated wavelength ratios of significant peaks and compared them to periodicity ratios of astronomical cycles at 560 Ma. These ratios match well with those listed in Table 1. Assuming wavelength peaks at 19.7 m (Interval 1), 31.4 m (Interval 2), 23.8 m (Interval 3), and 31.6 m (Interval 4) represent the long eccentricity signal, the other peaks would match short eccentricity, obliquity, and precession (Table 1). Hence, based on the assignment of significant spectral peaks to the long eccentricity cycle, the sedimentation rate is estimated to be 4.8 cm/kyr for Interval 1, 7.2 cm/kyr for Interval 2, 5.9 cm/kyr for Interval 3, and 7.3 cm/kyr for Interval 4 (Table 1).

The COCO analysis of the entire GR series suggests that sedimentation rates of 4.8, 6.0, 7.3, and 9.2 cm/kyr yield null hypothesis (H_0, no astronomical forcing) significance levels less than 0.01 (Fig. 4). The eCOCO analysis reflects variations of sedimentation rate throughout the GR series. The sedimentation rate varies between 4.8 and 7.3 cm/kyr, and, in general, is low in Intervals 1 and 3 and high in Intervals 2 and 4 (Fig. 4). The consistency of sedimentary rate estimates yielded by COCO and eCOCO analyses, and the correlation with the lithology support that our interpretation of significant spectral peaks to astronomical cycles is reliable.

4.2. Astrochronology

Because the 405-kyr long eccentricity is regarded as the most stable astronomical cycle in the Phanerozoic and has been proposed to have been recorded in rocks as old as 1.4 Ga (Zhang et al., 2015) and even 2.4 Ga (Lantink et al., 2019), it can serve as a "metronome" in astrochronological studies (Hinnov, 2013). To extract long eccentricity cycles, we applied Gaussian filters centered at 1/19.7, 1/31.4, 1/23.8, and 1/31.6 m^{-1} frequencies in four intervals, respectively (Fig. 5A). These cycles were tuned to the 405-kyr long eccentricity cycle (Fig. 5D), which enables an astronomical time scale to be constructed for the GR series and carbon isotope profile (Fig. 5). We also evaluated the sedimentation rate based on the 405-kyr tuned GR series. Similar patterns of sedimentation rate variation are observed in both eCOCO and 405-kyr tuned GR series results (Fig. 4B).

Using the sedimentation rate profile calibrated by 405-kyr cycles, the 460-m long SE in Oman spans 19 long eccentricity cycles (Fig. 5), which is 7.7 Myr in duration. Our results also indicate that the $\delta^{13}C$ values rapidly decrease to the nadir within three 405-kyr cycles ($\sim$ 1.2 Myr), and slowly return back in the following $\sim$ 6–7 Myr (Fig. 5). We considered three sources of uncertainties in our astrochronology: (1) the non-linear response of the paleoclimate to the astronomical forcing; (2) the stratigraphic levels of the onset and termination of the SE; and (3) the number of 405-kyr cycles encoded in the GR series. Firstly, by studying the Oligocene-Miocene deep-sea sediments, Zachos et al. (2001) suggested a fast response of the paleoclimate to astronomical forcing, and even for the slow-response proxies (e.g., $\delta^{18}O$ and $\delta^{13}C$), the phase lag to the 405-kyr eccentricity is within 10–15%. Here, we assign a total of $\pm$100 kyr uncertainty at the maximum considering the climate's response lag to the astronomical forcing. Secondly, the positions where the excursion initiated and terminated in the stratigraphy are pinpointed by the $\delta^{13}C$ data (Burns and Matter, 1993; Fike et al., 2006), which result in another $\pm$ 100 kyr uncertainty considering the sedimentation rate (Table 1) and the sampling interval of the $\delta^{13}C$ data ($\sim$ 2–6 m). Thirdly, we noticed a relatively sharp transition between Intervals 1 and 2 in the 405-kyr filter output (Fig. 5D), which is probably due to the change in the sedimentation rate at the lithological boundary. The phase offset between the 6th (E6) and the 7th (E7) 405-kyr cycle indicates the existence of the E7 cycle. Therefore, we argue that the number of 405 cycles is correctly counted. Taken together, the total duration of the SE is 7.7 $\pm$ 0.2 Myr.

A recent U-Pb zircon geochronology study from the Trepassey Formation in Newfoundland suggests that the termination age of the SE is 562.5 $\pm$ 1.1 Ma (Canfield et al., 2020), we could use it as an anchor point to constrain the termination age of the SE. Combining this radiometric age, the astrochronology of the SE yields a termination age of 570.2 $\pm$ 1.1 Ma for the excursion (Fig. 5E). The age uncertainty of 1.1 Ma is obtained from $\sqrt{1.1^2 + 0.2^2}$, propagated from the uncertainties of the anchor U-Pb age and the duration estimate.

5. Discussion

5.1. Astronomical forcing in the Shuram and Buah Formations

Astronomical forcing is regarded to be active throughout the Proterozoic and impose strong influences on Earth's climate (Zhang et al., 2015; Bao et al., 2018; Lantink et al., 2019). Our numerical analyses provided clear evidence for the encoding of astronomical signals in the Shuram and Buah Formations. We have identified a suite of astronomical cycles from the spectral analysis of the GR series, and have estimated the sedimentation rate based on the astronomical periodicities. Changes in sedimentation rate occur

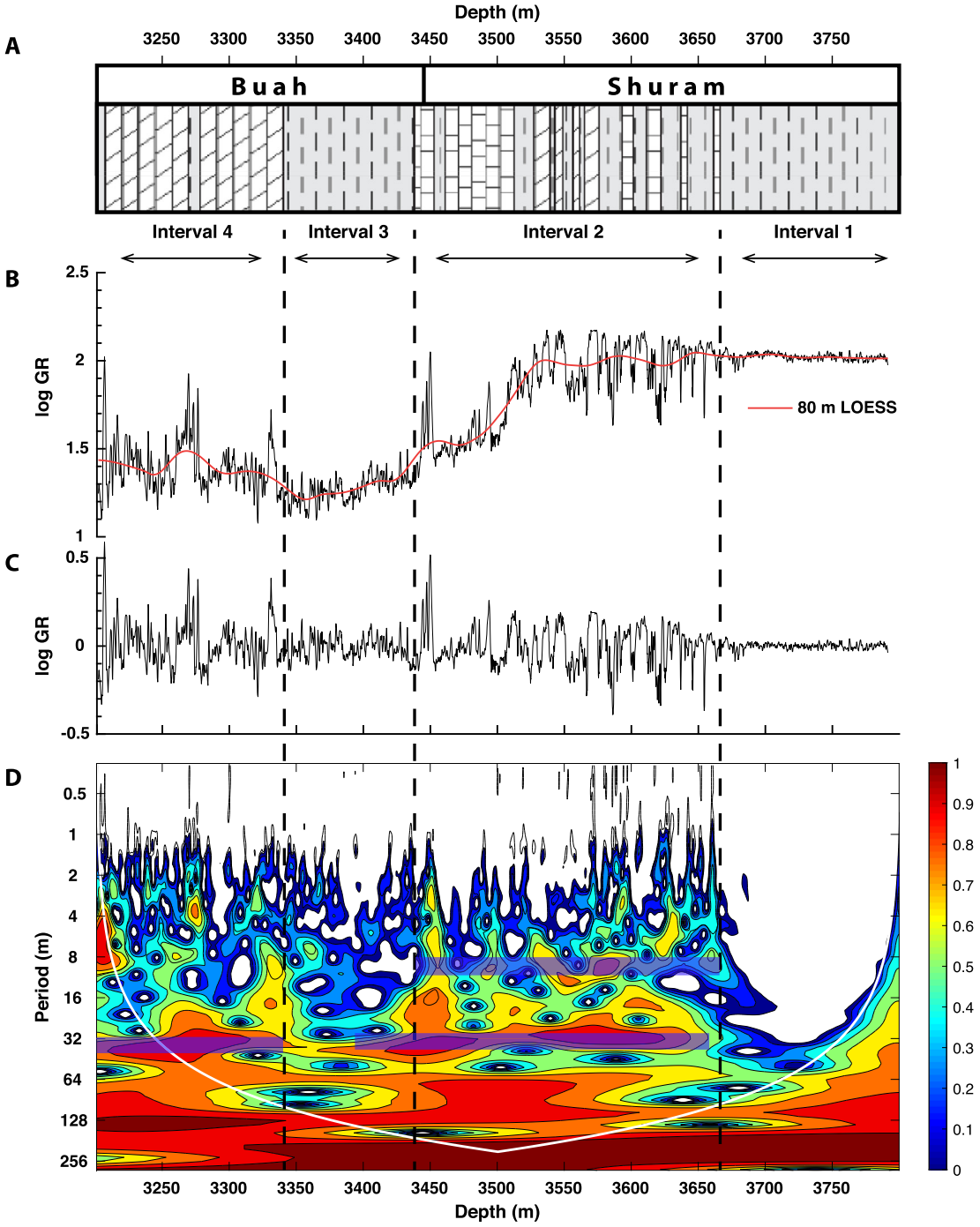

Fig. 2. (A) Lithology of the Shuram and Buah Formations. Four intervals are noted by arrows. (B) GR series after log-transformation (black) and its 80-m 'loess' long-term trend (red). (C) GR series after subtraction of the long-term trend. (D) Wavelet transform of GR series in (B). Area outside of the white line represents the "cone of influence", where edge effects become important. Shaded area (light blue) represents cyclicities with wavelengths of ~32 m and ~8 m.

at lithological boundaries, with low rates in shale-dominated layers and high rates in shale-carbonate interbedded layers (Fig. 4). The excellent correlation between sedimentation rate and lithology firmly supports the reliability of our estimates and the correct assignment of astronomical cycles. The low null hypothesis significance level of the COCO analysis suggests that the astronomical signals are accurately encoded in the GR series.

Paleoclimate could be influenced by astronomical forcing in many ways. For example, the astronomical control on the fluctuations in the ice volume and sea level in the Pliocene and Pleistocene is well established by marine $\delta^{18}O$ records from deep-sea cores (Lisiecki and Raymo, 2005). Besides, studies have shown that the long-term migration of the Intertropical Convergence Zone (ITCZ) varies at astronomical time scale (Wang et al., 2004; Liu et al., 2015), which strongly dominates the intensity and distribution of tropical precipitation.

The encoding mechanism of astronomical cycles in the Shuram and Buah Formations is likely a combination of changes in both the sea level and the position of the ITCZ. During Ediacaran time, Oman was located in or very close to the tropics (Kempf et al., 2000; Kilner et al., 2005), so it is sensitive to the migration of the ITCZ. Astronomical forcing modulated the position shift of the ITCZ and hence resulted in the fluctuation of monsoon intensities and runoff fluxes. When ITCZ was close to the Oman, terrestrial input

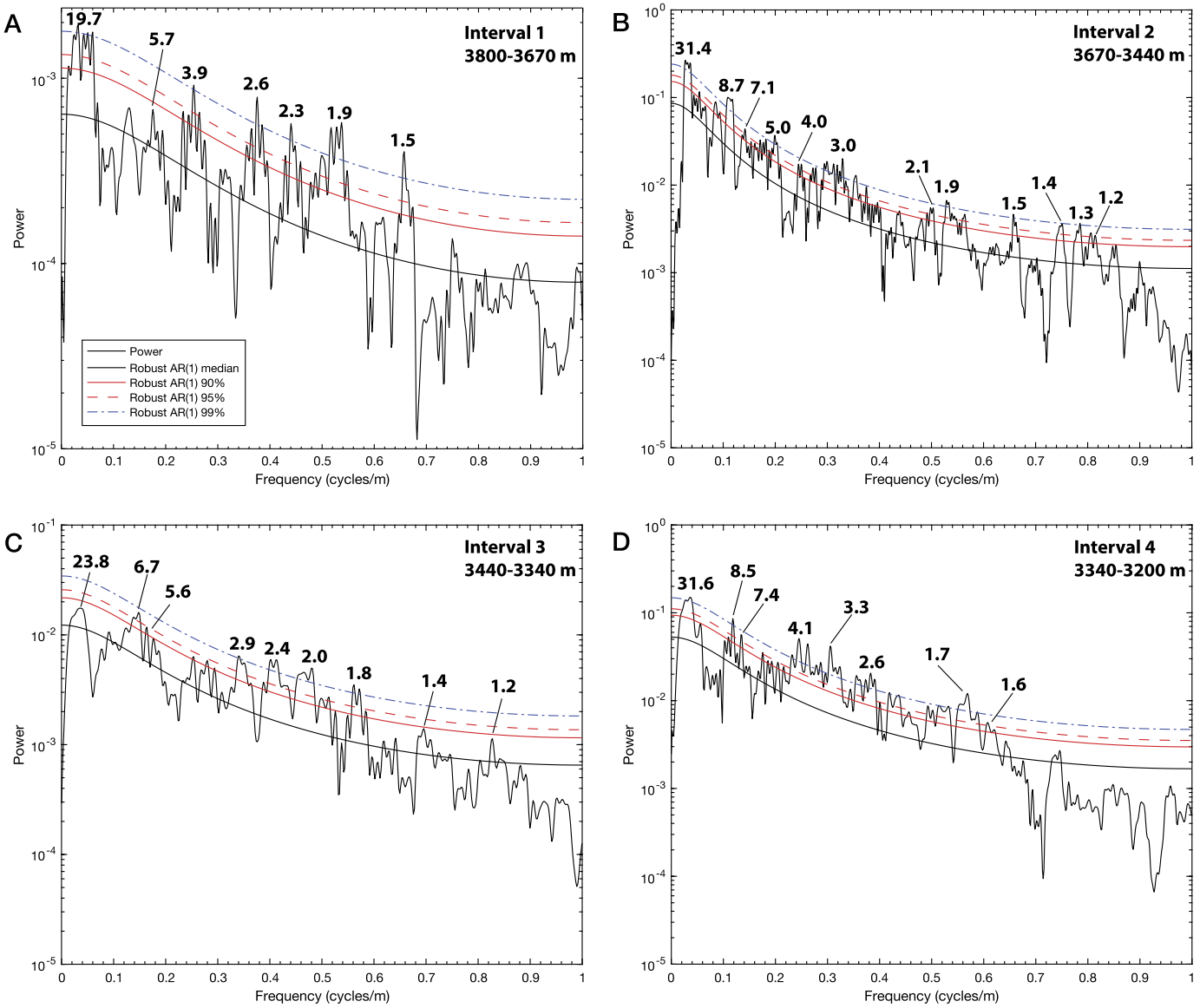

Fig. 3. 2π MTM power spectra of (A) Interval 1 (3800–3670 m), (B) Interval 2 (3670–3440 m), (C) Interval 3 (3440–3340 m), and (D) Interval 4 (3340–3200 m). Significant peaks are shown with robust AR(1) model, and 90%, 95%, and 99% confidence levels. Significant peaks are marked with their corresponding wavelengths in meters.

into the ocean would be intensified, which brought more clay minerals for sedimentation, hence, higher GR values. In the opposite scenario, less clay input would cause lower GR values. Besides, the waxing and waning of the ice volume influenced by astronomical cycles would cause sea level variations, which changes the depositional environments and results in the alternating carbonate and terrigenous deposition.

5.2. Global synchroneity the SE and its implications

The duration of the SE in the Miqrat-1 Well is estimated to be 7.7 ± 0.2 Myr. We compared this result with duration estimates by astrochronology from other exposures of the SE globally (Fig. 6). For instance, an 8.0 ± 0.5 Myr duration was obtained from the Wonoka Formation, South Australia (Minguez and Kodama, 2017). Likewise, Gong et al. (2017) suggested a 9.1 ± 1.0 Myr duration from the Doushantuo Formation, South China. Minguez et al. (2015) published an 8.2 ± 1.2 Myr duration from the Johnnie Formation in the United States. By adding the result from Oman, we now have a paleogeographically broader coverage of the SE, with sections from all major basins worldwide. The consistency of these duration estimates strongly argues for the global synchroneity of the SE. Besides, because of the high-resolution astrochronology, we were able to calculate the time interval between the onset of the excursion and the nadir of the $\delta^{13}C$ values in Oman and South Australia. These two widely separated sections both show that the excursion reaches its nadir value in about 1.0–1.2 Myr (Fig. 6). Moreover, the same geomagnetic reversal that was identified right at the nadir of the SE in sections from South Australia and the United States also indicates that the SE was globally synchronous (Fig. 6; Minguez and Kodama, 2017). Therefore, we suggest that, rather than being a locally diagenetic overprint (e.g., Derry, 2010), the SE has a primary origin and the depleted $\delta^{13}C$ values are probably a global signature.

The primary origin of the SE requires a mechanism that can explain the unprecedented perturbation of the Ediacaran carbon cycle. It is hypothesized that there was a large dissolved organic carbon (DOC) reservoir suspended in the anoxic Ediacaran ocean, and the oxygenation of that DOC reservoir would release a large amount of ^{12}C from organic carbon, and could produce depleted carbon isotope values (Fike et al., 2006). Geochemical studies, particularly focusing on the redox-sensitive trace metals and their

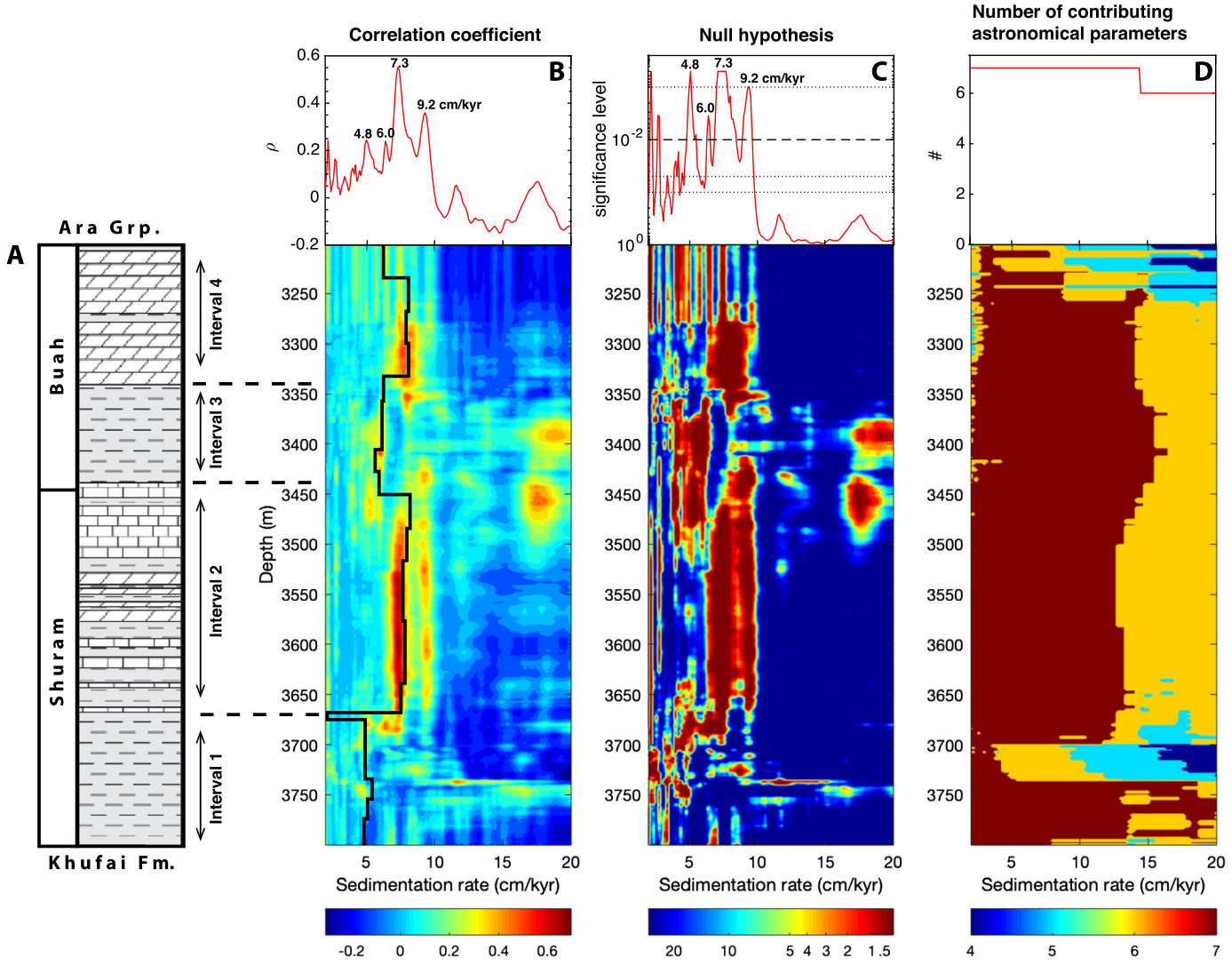

Fig. 4. Results of the COCO and eCOCO analyses compared with the lithology of the Miqrat-1 Well. (A) Lithological column of the Shuram and Buah Formations (modified from Bowring et al., 2007). (B) Correlation coefficient (top) and evolutionary correlation coefficient (bottom). (C) Null hypothesis (H_0, no astronomical forcing; top) and evolutionary H_0 significance level (bottom). (D) The number of contributing astronomical parameters (top) and evolutionary number of contributing astronomical parameters (bottom). Number of Monte Carlo simulations is 2000. Sedimentation rates range from 2 to 20 cm/kyr with an increasing step of 0.1 cm/kyr. The sliding window size is 149.7 m; the sliding window step is 0.15 m. Potential sedimentation rates are shown in numbers with H_0 significance level less than 0.01. Black solid lines represent the sedimentation rate calculated from the 405-kyr tuned GR series.

isotopes, support that a global ocean oxygenation event occurred broadly coeval to the SE (Sahoo et al., 2016). Specifically, a recent uranium isotope study of the SE in South China, Siberia, and the United States suggests that the ocean was extensively oxygenated to a degree comparable to near-modern levels (Zhang et al., 2019). In order to sustain the oxygenation of such a large DOC reservoir, an enormous amount of oxidant is required. The exact amount of the DOC is dependent on the duration of the SE. For example, Bristow and Kennedy (2008) argued that the available oxidant during the Ediacaran time could not sustain a 25–50 Myr long excursion. Our 7.7 ± 0.2 Myr estimate, however, does largely reduce the amount of required oxidant, and provide a new boundary condition for future geochemical models.

Previously, the termination age of the SE was considered to be 551.1 ± 0.7 Ma, which is obtained by the ID-TIMS U-Pb geochronology on zircons from an ash layer in the Dengying Formation, South China (Condon et al., 2005). However, the ash layer Condon et al. (2005) sampled is in the lower Dengying Formation, which is unconformably above the SE (Fig. 6). Instead, Zhou et al. (2018) dated a K-bentonite layer from the lowermost Dengying Formation, which constrains the SE to be older than 557 ± 3 Ma (Fig. 6). Moreover, the carbon isotope record from the Trepassey Formation in Newfoundland is suggested to be equivalent to the SE. Based on this correlation, a U-Pb zircon age from an ash layer of the Trepassey Formation constrains the termination age to be 562.5 ± 1.1 Ma (Canfield et al., 2020). When combined with our astrochronology, the onset age of the SE is 570.2 ± 1.1 Ma.

Within the new astrochronological framework, the temporal links between the Ediacaran global carbon cycle, the paleoclimate, and biological changes could be evaluated. Our new age constraints on the SE could also facilitate stratigraphic correlation between sections where there are sparse $\delta^{13}C$ data but good ages and phenomenal fossil records (e.g., Newfoundland), or places with no or very few age constraints but with a well-defined carbon isotope profile (e.g., Siberia, India). According to our age estimates, the onset of the SE is 570.2 ± 1.1 Ma, ~ 10 Myr younger than the ca. 580 Ma Gaskiers glaciation (Pu et al., 2016), thus, ruling out the temporal link between the excursion and the Gaskiers glaciation that is previously proposed by Al-Husseini (2014). However, there is a close timing between the onset of the SE and the evolution of the

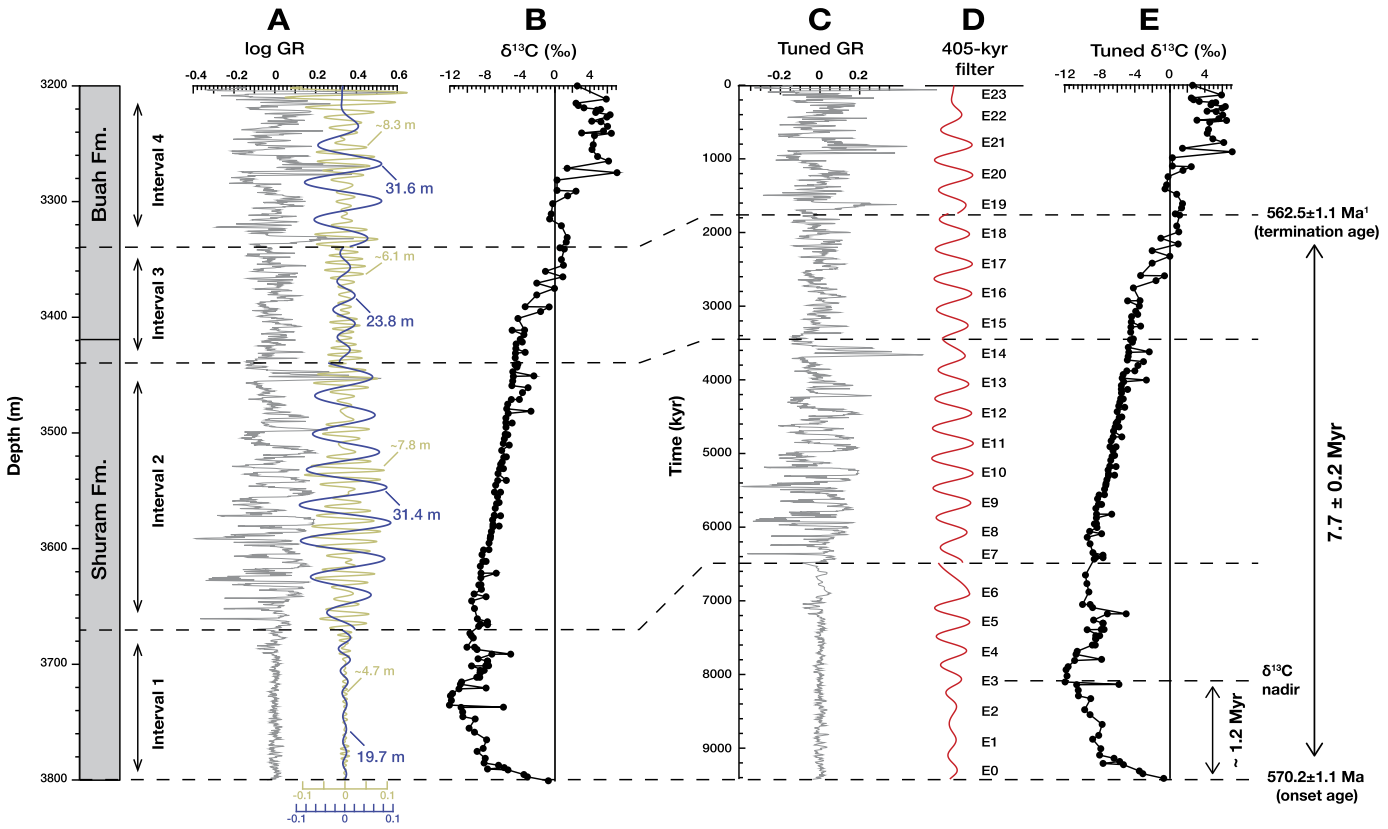

Fig. 5. (A) The detrended GR series shown with Gaussian filter outputs of interpreted long (blue) and short (brown) eccentricity cycles (passbands: 0.0317 ± 0.0063, 0.420 ± 0.0084, 0.0318 ± 0.0064, and 0.0508 ± 0.010 cycles/m for Intervals 1, 2, 3, and 4, respectively). (B) Carbon isotope profile of the Shuram and Buah Formations (Burns and Matter, 1993; Fike et al., 2006). (C) 405-kyr tuned detrended GR series. (D) Standardized 405-kyr long eccentricity cycles filtered outputs (passband: 0.00247 ± 0.0002 cycles/kyr). (E) 405-kyr eccentricity tuned carbon isotope profile. Termination age of the SE is correlated to the U-Pb age from (1) Canfield et al. (2020).

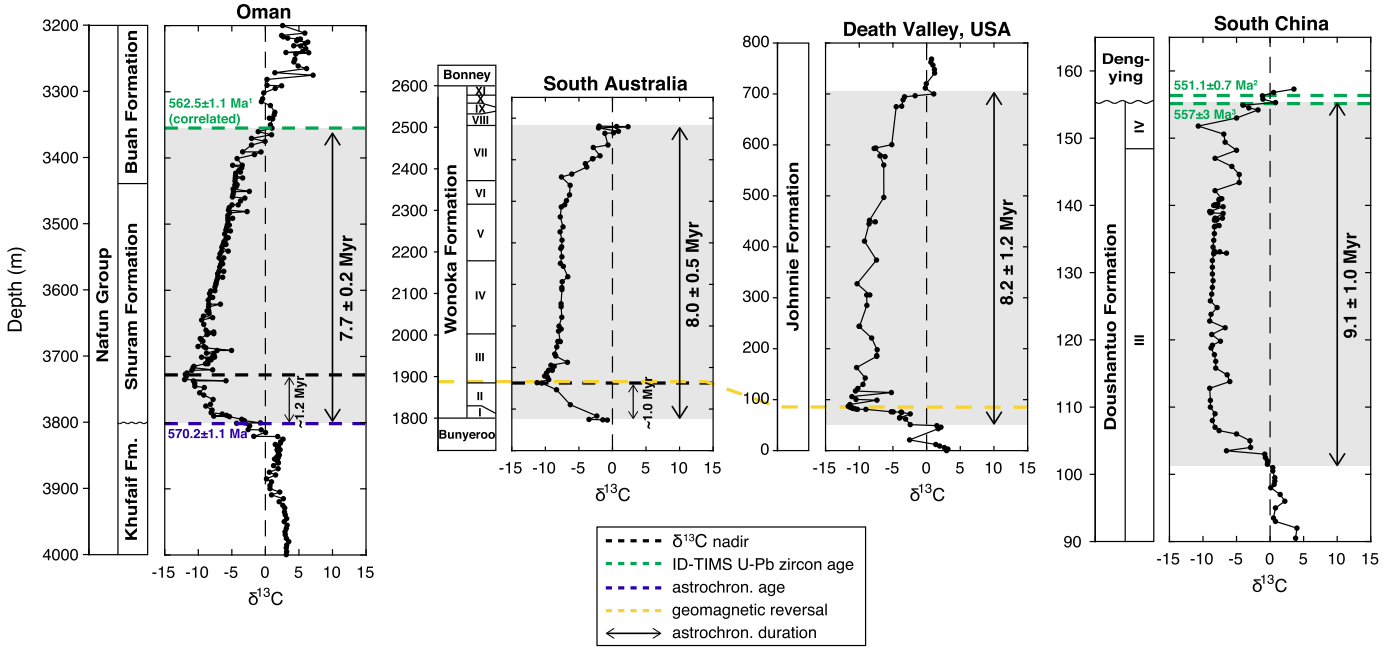

Fig. 6. Composite chrono- and chemo-stratigraphy of the type sections from Oman, Flinders Ranges, South Australia, Death Valley, USA, and South China. Carbon isotope, astrochronological, and geomagnetic reversal data sources: Oman (Burns and Matter, 1993; Fike et al., 2006), South Australia (Calver, 2000; Minguez and Kodama, 2017), the United States (Verdel et al., 2011; Minguez et al., 2015), and South China (Condon et al., 2005; McFadden et al., 2008; Gong et al., 2017). U-Pb zircon ages are from (1) Canfield et al. (2020), (2) Condon et al. (2005), and (3) Zhou et al. (2018).

Ediacaran biota. In Newfoundland, the Avalon assemblage is identified immediately above the 570.9 ± 0.4 Ma Drook Formation (Narbonne and Gehling, 2003; Pu et al., 2016), largely overlapping with the SE. The following diversification of the White Sea assemblage (558 ± 1 Ma; 559.3 ± 2 Ma; Grazhdankin, 2004) slightly postdates the termination of the carbon isotope excursion. Assuming

the SE is originated from the oxygenation of the marine DOC, the final exhaustion of this large DOC reservoir might provide a well oxygenated ocean for the Ediacara biota to evolve. The astronomically calibrated time scale for the SE permits further investigations on the dynamic interactions between the global carbon cycle, the evolution of the Ediacara biota, and the redox landscapes of the ocean in the latest Neoproterozoic.

6. Conclusions

Precisely constraining the age and the duration of the SE is important in order to understand the origin of this unprecedented perturbation in the global carbon cycle in Ediacaran time. The Miqrat-1 Well from Oman provides an excellent sedimentary sequence of the Nafun Group, in which the SE is completely recorded in the Shuram and Buah Formations. Power spectral analysis of the GR log from the Miqrat-1 Well reveals a hierarchy of cyclicities. Based on the sedimentation rate we estimate, these cyclicities correspond with astronomically-forced climate cycles (eccentricity, obliquity, and precession) that are accurately encoded in the GR series. The eCOCO and 405-kyr tuned GR series permit a record of sedimentation rate variations throughout the Shuram and Buah Formations. Results show that sedimentation rate and lithology are well-correlated, with low rates in shale-dominated layers and high rates in shale-carbonate interbedded layers. The established astrochronology constrains the duration of the SE to be 7.7 $\pm$ 0.2 Myr in Oman, which is consistent with the $\sim$ 8 Myr estimates from exposures in South Australia, South China, and the United States. Hence, we provided supporting evidence for the global synchroneity of the SE that argues for a primary origin for the depleted $\delta^{13}C$ values. Combined with existing radiometric ages and stratigraphic correlations, the onset and the termination ages of the SE are 570.2 $\pm$ 1.1 Ma and 562.5 $\pm$ 1.1 Ma, respectively. We also suggested that the rhythm of the excursion is characterized by a fast decline in $\delta^{13}C$ values, reaching to the nadir within $\sim$ 1 Myr, and a slow shift back in the following $\sim$ 6–7 Myr. The high-resolution astrochronology of the SE bears significant implications for testing the temporal and causal links between the global carbon cycle and the broadly contemporaneous paleoclimate and biological events in the latest Neoproterozoic, e.g., the Gaskiers glaciation, the extensive oceanic oxygenation, and the evolution of the Ediacara biota.

CRediT authorship contribution statement

Zheng Gong: Conceptualization, Formal analysis, Methodology, Visualization, Writing - original draft. **Mingsong Li:** Methodology, Software, Visualization, Writing - original draft.

Declaration of competing interest

The authors declare that they have no known competing financial interests or personal relationships that could have appeared to influence the work reported in this paper.

Acknowledgements

Zheng Gong was supported by the Graduate Student Fellowship from Yale University. Mingsong Li was supported by the Heising-Simons Foundation, United States (2016–11). We thank Moujahed Al-Husseini and GeoArabia for permission to use the data, Lei Xu for data collection, and David Evans, Alan Rooney, and Ross Mitchell for helpful discussions. Critiques from the editor and two reviewers led to an improved manuscript.

Appendix A. Supplementary material

Supplementary material related to this article can be found online at https://doi.org/10.1016/j.epsl.2020.116462.

References

Al-Husseini, M.I., 2014. Proposed correlation of Oman's Abu Mahara Supergroup and Saudi Arabia's Jibalah Group. GeoArabia 19 (2), 17–48.
Bao, X., Zhang, S., Jiang, G., Wu, H., Li, H., Wang, X., et al., 2018. Cyclostratigraphic constraints on the duration of the Datangpo Formation and the onset age of the Nantuo (Marinoan) glaciation in South China. Earth Planet. Sci. Lett. 483, 52–63.
Berger, A., Loutre, M.F., 1994. Astronomical forcing through geological time. In: De Boer, P.L., Smith, D.G. (Eds.), Orbital Forcing and Cyclic Sequences, vol. 19. Blackwell Scientific Publications, Oxford, pp. 15–24.
Bjerrum, C.J., Canfield, D.E., 2011. Towards a quantitative understanding of the late Neoproterozoic carbon cycle. Proc. Natl. Acad. Sci. 108 (14), 5542–5547.
Bowring, S.A., Grotzinger, J.P., Condon, D.J., Ramezani, J., Newall, M.J., Allen, P.A., 2007. Geochronologic constraints on the chronostratigraphic framework of the Neoproterozoic Huqf Supergroup, Sultanate of Oman. Am. J. Sci. 307 (10), 1097–1145.
Bristow, T.F., Kennedy, M.J., 2008. Carbon isotope excursions and the oxidant budget of the Ediacaran atmosphere and ocean. Geology 36 (11), 863–866.
Burns, S.J., Matter, A., 1993. Carbon isotopic record of the latest Proterozoic from Oman. Eclogae Geol. Helv. 86 (2), 595–607.
Butterfield, N.J., Grotzinger, J.P., 2012. Palynology of the Huqf Supergroup, Oman. Geol. Soc. (Lond.) Spec. Publ. 366 (1), 251–263.
Calver, C.R., 2000. Isotope stratigraphy of the Ediacarian (Neoproterozoic III) of the Adelaide Rift Complex, Australia, and the overprint of water column stratification. Precambrian Res. 100 (1–3), 121–150.
Canfield, D.E., Knoll, A.H., Poulton, S.W., Narbonne, G.M., Dunning, G.R., 2020. Carbon isotopes in clastic rocks and the Neoproterozoic carbon cycle. Am. J. Sci. 320 (2), 97–124.
Condon, D., Zhu, M., Bowring, S., Wang, W., Yang, A., Jin, Y., 2005. U-Pb ages from the Neoproterozoic Doushantuo Formation, China. Science 308 (5718), 95–98.
Corsetti, F.A., Kaufman, A.J., 2003. Stratigraphic investigations of carbon isotope anomalies and Neoproterozoic ice ages in Death Valley, California. Geol. Soc. Am. Bull. 115 (8), 916–932.
Derry, L.A., 2010. A burial diagenesis origin for the Ediacaran Shuram-Wonoka carbon isotope anomaly. Earth Planet. Sci. Lett. 294 (1–2), 152–162.
Fike, D.A., Grotzinger, J.P., Pratt, L.M., Summons, R.E., 2006. Oxidation of the Ediacaran ocean. Nature 444 (7120), 744–747.
Forbes, G.A., Jansen, H.S., Schreurs, J., 2010. Lexicon of Oman: Subsurface Stratigraphy: Reference Guide to the Stratigraphy of Oman's Hydrocarbon Basins. Gulf PetroLink.
Gong, Z., Kodama, K.P., Li, Y.X., 2017. Rock magnetic cyclostratigraphy of the Doushantuo Formation, South China and its implications for the duration of the Shuram carbon isotope excursion. Precambrian Res. 289, 62–74.
Gong, Z., Kodama, K.P., Li, Y.X., 2019. Paleomagnetism and rock magnetic cyclostratigraphy of the Ediacaran Doushantuo Formation, South China: constraints on the remagnetization mechanism and the encoding process of Milankovitch cycles. Palaeogeogr. Palaeoclimatol. Palaeoecol. 528, 232–246.
Gorin, G.E., Racz, L.G., Walter, M.R., 1982. Late Precambrian-Cambrian sediments of Huqf Group, Sultanate of Oman. AAPG Bull. 66 (12), 2609–2627.
Grazhdankin, D., 2004. Patterns of distribution in the Ediacaran biotas: facies versus biogeography and evolution. Paleobiology 30 (2), 203–221.
Grotzinger, J.P., Fike, D.A., Fischer, W.W., 2011. Enigmatic origin of the largest-known carbon isotope excursion in Earth's history. Nat. Geosci. 4 (5), 285.
Halverson, G.P., Hoffman, P.F., Schrag, D.P., Maloof, A.C., Rice, A.H.N., 2005. Toward a Neoproterozoic composite carbon-isotope record. Geol. Soc. Am. Bull. 117 (9–10), 1181–1207.
Hinnov, L.A., 2013. Cyclostratigraphy and its revolutionizing applications in the Earth and planetary sciences. Geol. Soc. Am. Bull. 125 (11–12), 1703–1734.
Kempf, O., Kellerhals, P., Lowrie, W., Matter, A., 2000. Paleomagnetic directions in late Precambrian glaciomarine sediments of the Mirbat Sandstone Formation, Oman. Earth Planet. Sci. Lett. 175 (3–4), 181–190.
Kilner, B., Niocaill, C., Brasier, M., 2005. Low-latitude glaciation in the Neoproterozoic of Oman. Geology 33 (5), 413–416.
Knoll, A., Walter, M., Narbonne, G., Christie-Blick, N., 2006. The Ediacaran Period: a new addition to the geologic time scale. Lethaia 39 (1), 13–30.
Kump, L.R., Arthur, M.A., 1999. Interpreting carbon-isotope excursions: carbonates and organic matter. Chem. Geol. 161 (1–3), 181–198.
Lantink, M.L., Davies, J.H., Mason, P.R., Schaltegger, U., Hilgen, F.J., 2019. Climate control on banded iron formations linked to orbital eccentricity. Nat. Geosci. 12 (5), 369–374.
Laskar, J., Robutel, P., Joutel, F., Gastineau, M., Correia, A.C.M., Levrard, B., 2004. A long-term numerical solution for the insolation quantities of the Earth. Astron. Astrophys. 428 (1), 261–285.

Le Guerroué, E., Allen, P.A., Cozzi, A., Etienne, J.L., Fanning, M., 2006. 50 Myr recovery from the largest negative $\delta^{13}C$ excursion in the Ediacaran ocean. Terra Nova 18 (2), 147–153.

Lee, C., Fike, D.A., Love, G.D., Sessions, A.L., Grotzinger, J.P., Summons, R.E., Fischer, W.W., 2013. Carbon isotopes and lipid biomarkers from organic-rich facies of the Shuram Formation, Sultanate of Oman. Geobiology 11 (5), 406–419.

Li, M., Kump, L.R., Hinnov, L.A., Mann, M.E., 2018. Tracking variable sedimentation rates and astronomical forcing in Phanerozoic paleoclimate proxy series with evolutionary correlation coefficients and hypothesis testing. Earth Planet. Sci. Lett. 501, 165–179.

Li, M., Hinnov, L., Kump, L., 2019a. Acycle: time-series analysis software for paleoclimate research and education. Comput. Geosci. 127, 12–22.

Li, M., Huang, C., Ogg, J., Zhang, Y., Hinnov, L., Wu, H., et al., 2019b. Paleoclimate proxies for cyclostratigraphy: comparative analysis using a Lower Triassic marine section in South China. Earth-Sci. Rev. 189, 125–146.

Lisiecki, L.E., Raymo, M.E., 2005. A Pliocene-Pleistocene stack of 57 globally distributed benthic $\delta^{18}O$ records. Paleoceanography 20 (1).

Liu, Y., Lo, L., Shi, Z., Wei, K.Y., Chou, C.J., Chen, Y.C., et al., 2015. Obliquity pacing of the western Pacific Intertropical Convergence Zone over the past 282,000 years. Nat. Commun. 6 (1), 1–7.

Lyons, T.W., Reinhard, C.T., Planavsky, N.J., 2014. The rise of oxygen in Earth's early ocean and atmosphere. Nature 506 (7488), 307.

Mann, M.E., Lees, J.M., 1996. Robust estimation of background noise and signal detection in climatic time series. Clim. Change 33 (3), 409–445.

McFadden, K.A., Huang, J., Chu, X., Jiang, G., Kaufman, A.J., Zhou, C., et al., 2008. Pulsed oxidation and biological evolution in the Ediacaran Doushantuo Formation. Proc. Natl. Acad. Sci. 105 (9), 3197–3202.

Meert, J.G., Levashova, N.M., Bazhenov, M.L., Landing, E., 2016. Rapid changes of magnetic field polarity in the late Ediacaran: linking the Cambrian evolutionary radiation and increased UV-B radiation. Gondwana Res. 34, 149–157.

Minguez, D., Kodama, K.P., Hillhouse, J.W., 2015. Paleomagnetic and cyclostratigraphic constraints on the synchroneity and duration of the Shuram carbon isotope excursion, Johnnie Formation, Death Valley Region, CA. Precambrian Res. 266, 395–408.

Minguez, D., Kodama, K.P., 2017. Rock magnetic chronostratigraphy of the Shuram carbon isotope excursion: Wonoka Formation, Australia. Geology 45 (6), 567–570.

Miyazaki, Y., Planavsky, N.J., Bolton, E.W., Reinhard, C.T., 2018. Making sense of massive carbon isotope excursions with an inverse carbon cycle model. J. Geophys. Res., Biogeosci. 123 (8), 2485–2496.

Narbonne, G.M., Gehling, J.G., 2003. Life after snowball: the oldest complex Ediacaran fossils. Geology 31 (1), 27–30.

Pisarevsky, S.A., Murphy, J.B., Cawood, P.A., Collins, A.S., 2008. Late Neoproterozoic and Early Cambrian palaeogeography: models and problems. Geol. Soc. (Lond.) Spec. Publ. 294 (1), 9–31.

Pu, J.P., Bowring, S.A., Ramezani, J., Myrow, P., Raub, T.D., Landing, E., et al., 2016. Dodging snowballs: geochronology of the Gaskiers glaciation and the first appearance of the Ediacaran biota. Geology 44 (11), 955–958.

Sahoo, S.K., Planavsky, N.J., Jiang, G., Kendall, B., Owens, J.D., Wang, X., et al., 2016. Oceanic oxygenation events in the anoxic Ediacaran ocean. Geobiology 14 (5), 457–468.

Torrence, C., Compo, G.P., 1998. A practical guide to wavelet analysis. Bull. Am. Meteorol. Soc. 79 (1), 61–78.

Thomson, D.J., 1982. Spectrum estimation and harmonic analysis. Proc. IEEE 70 (9), 1055–1096.

Verdel, C., Wernicke, B.P., Bowring, S.A., 2011. The Shuram and subsequent Ediacaran carbon isotope excursions from southwest Laurentia, and implications for environmental stability during the metazoan radiation. Geol. Soc. Am. Bull. 123 (7–8), 1539–1559.

Waltham, D., 2015. Milankovitch period uncertainties and their impact on cyclostratigraphy. J. Sediment. Res. 85 (8), 990–998.

Wang, X., Auler, A.S., Edwards, R.L., Cheng, H., Cristalli, P.S., Smart, P.L., et al., 2004. Wet periods in northeastern Brazil over the past 210 kyr linked to distant climate anomalies. Nature 432 (7018), 740–743.

Weedon, G.P., 2005. Time-Series Analysis and Cyclostratigraphy: Examining Stratigraphic Records of Environmental Cycles. Cambridge University Press.

Witkosky, R., Wernicke, B.P., 2018. Subsidence history of the Ediacaran Johnnie Formation and related strata of southwest Laurentia: implications for the age and duration of the Shuram isotopic excursion and animal evolution. Geosphere 14 (5), 2245–2276.

Xiao, S., Laflamme, M., 2009. On the eve of animal radiation: phylogeny, ecology and evolution of the Ediacara biota. Trends Ecol. Evol. 24 (1), 31–40.

Zachos, J.C., Shackleton, N.J., Revenaugh, J.S., Pälike, H., Flower, B.P., 2001. Climate response to orbital forcing across the Oligocene-Miocene boundary. Science 292 (5515), 274–278.

Zhang, F., Xiao, S., Romaniello, S.J., Hardisty, D., Li, C., Melezhik, V., et al., 2019. Global marine redox changes drove the rise and fall of the Ediacara biota. Geobiology 17 (6), 594–610.

Zhang, S., Wang, X., Hammarlund, E.U., Wang, H., Costa, M.M., Bjerrum, C.J., et al., 2015. Orbital forcing of climate 1.4 billion years ago. Proc. Natl. Acad. Sci. 112 (12), E1406–E1413.

Zhou, M., Luo, T., Huff, W.D., Yang, Z., Zhou, G., Gan, T., et al., 2018. Timing the termination of the Doushantuo negative carbon isotope excursion: evidence from U-Pb ages from the Dengying and Liuchapo formations, South China. Sci. Bull. 63 (21), 1431–1438.